Chemical Science

ROYAL SOCIETY OF CHEMISTRY

EDGE ARTICLE

View Article Online
View Journal | View Issue

Cite this: *Chem. Sci.*, 2022, **13**, 3489

All publication charges for this article have been paid for by the Royal Society of Chemistry

Received 17th November 2021
Accepted 28th February 2022

DOI: 10.1039/d1sc06418e

rsc.li/chemical-science

A conformational role for NifW in the maturation of molybdenum nitrogenase P-cluster†

Casey Van Stappen, ‡[a] Emilio Jiménez-Vicente,‡[b] Ana Pérez-González, [b] Zhi-Yong Yang,[c] Lance C. Seefeldt, [c] Serena DeBeer, [a] Dennis R. Dean[b] and Laure Decamps *[a]

Reduction of dinitrogen by molybdenum nitrogenase relies on complex metalloclusters: the [8Fe:7S] P-cluster and the [7Fe:9S:Mo:C:homocitrate] FeMo-cofactor. Although both clusters bear topological similarities and require the reductive fusion of [4Fe:4S] sub-clusters to achieve their respective assemblies, P-clusters are assembled directly on the $NifD_2K_2$ polypeptide prior to the insertion of FeMo-co, which is fully assembled separately from $NifD_2K_2$. P-cluster maturation involves the iron protein $NifH_2$ as well as several accessory proteins, whose role has not been elucidated. In the present work, two $NifD_2K_2$ species bearing immature P-clusters were isolated from an *Azotobacter vinelandii* strain in which the genes encoding NifH and the accessory protein NifZ were deleted, and characterized by X-ray absorption spectroscopy and EPR. These analyses showed that both $NifD_2K_2$ complexes harbor clusters that are electronically and structurally similar, with each NifDK unit containing two $[4Fe:4S]^{2+/+}$ clusters. Binding of the accessory protein NifW parallels a decrease in the distance between these clusters, as well as a subtle change in their coordination. These results support a conformational role for NifW in P-cluster biosynthesis, bringing the two [4Fe:4S] precursors closer prior to their fusion, which may be crucial in challenging cellular contexts.

Introduction

Nitrogenases are the catalytic components of biological nitrogen fixation, achieving the nucleotide-dependent reduction of dinitrogen (N_2) to ammonia (NH_3) at ambient temperature and pressure.[1–3] Three structurally and functionally similar but genetically distinct types of nitrogenases have been identified, which are classified according to the heterometal (Mo, V) or lack thereof (Fe) of their cofactors. All microbial nitrogen fixers identified to date produce at least Mo nitrogenase, and certain also produce either or both V- and Fe nitrogenase.[4] Mo nitrogenase is composed of catalytic components that include a homodimeric Fe protein, encoded by *nifH*, and a heterotetrameric MoFe protein, encoded by *nifD* and *nifK*. For clarity and consistency, in the present work a nomenclature derived from the corresponding genes will be used to designate the catalytic components as well as certain other proteins involved in maturation of the MoFe protein. For example, Fe protein is designated $NifH_2$ and the MoFe protein is designated $NifD_2K_2$ (subscripts indicate subunit organization). $NifH_2$ contains two MgATP-binding sites and a single redox active [4Fe:4S] cluster that sequentially supplies electrons to $NifD_2K_2$. $NifD_2K_2$ harbors two pairs of complex metalloclusters that participate in catalysis: the [8Fe:7S] P-cluster and the [7Fe:9S:Mo:C:homocitrate] FeMo-cofactor (FeMo-co).[3] The P-cluster is located between the subunits of each NifDK catalytic unit and is involved in the inter- and intra-component delivery of electrons from the $NifH_2$ [4Fe:4S] cluster to FeMo-co, which provides the site for substrate binding and reduction.[3,5,6] Understanding the biosynthesis of nitrogenase metalloclusters is crucial from the practical perspective of endowing certain eukaryotes the capacity to fix nitrogen by transferring the genetic determinants from diazotrophs, as well as for improving the nitrogen fixing capacity of symbiotic nitrogen fixing microbes associated with crop plants.[7–10]

There is some topological similarity between the P-cluster and FeMo-co (Fig. 1) as their [Fe:S] cores can be considered to represent fused or bridged sub-cluster units. Recent refinement of a structural model of NifB, involved in formation of the [Fe:S:C] core common to all three nitrogenase cofactors, suggested a P-cluster-like intermediate as FeMo-co precursor during its formation.[11] Nevertheless, there is a fundamental difference between FeMo-co assembly and P-cluster maturation.

[a]*Max Planck Institute for Chemical Energy Conversion, Stiftstrasse 34-36, 45470 Mülheim an der Ruhr, Germany. E-mail: laure.decamps@cec.mpg.de*

[b]*Department of Biochemistry, Virginia Polytechnic Institute and State University, Blacksburg, VA 24061, USA*

[c]*Department of Chemistry and Biochemistry, Utah State University, Logan, UT 84322, USA*

† Electronic supplementary information (ESI) available: Experimental procedures, supplementary figures and tables. See DOI: 10.1039/d1sc06418e

‡ C. V. S. and E. J. V. contributed equally to this work.

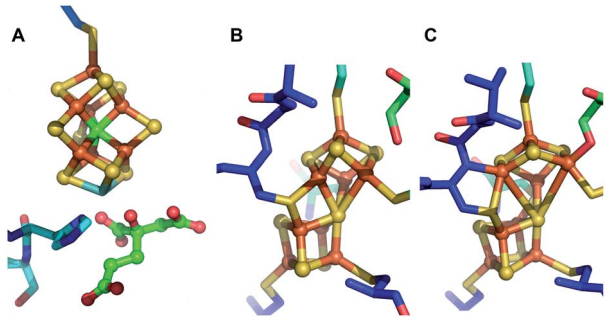

Fig. 1 Structures of the [Fe:S] clusters of $NifD_2K_2$ of *A. vinelandii*. (A) FeMo-co in DT-reduced $NifD_2K_2$ (PDB ID: 3U7Q); (B) P-cluster in the resting all-ferrous P^N state (PDB ID: 3MIN); (C) P-cluster in the 2-electron oxidized P^{2+} state (PDB ID: 2MIN).[15]

FeMo-co is separately assembled on a series of scaffolds and subsequently inserted into an immature form of $NifD_2K_2$, designated apo-$NifD_2K_2$, which already contains mature P-clusters.[9,12] In contrast, it appears that an earlier stage of $NifD_2K_2$ maturation involves formation of a P-cluster precursor directly within the polypeptide, which is then processed to apo-$NifD_2K_2$ replete with mature P-clusters. In the case of Mo nitrogenase of *Azotobacter vinelandii*, P-cluster maturation involves the interaction of immature forms of $NifD_2K_2$ with the dispensable accessory proteins NafH, NifW and NifZ.[13,14] P-cluster maturation within $NifD_2K_2$ also obligately requires the other nitrogenase catalytic component, $NifH_2$, and MgATP.[16–18] The prevailing model for P-cluster maturation is that two [4Fe:4S] clusters are separately formed within opposing NifD and NifK subunits, representing a P-cluster precursor, and then fused in a process involving elimination of a single S atom from one of the [4Fe:4S] units. Although it has been clearly established that each P-cluster precursor contains 8 iron atoms, it is not possible to accurately quantify the S content of P-cluster precursors. It is therefore not possible to distinguish whether P-cluster precursors represent separately paired [4Fe:4S] clusters or an [8Fe:7S] cluster that has already tethered two [4Fe:4S] units together through a shared central S atom. Such a species would be expected to have the same chemical composition as mature P-cluster but differ by some combination of differing redox state, conformation, and/or ligand arrangement.

Besides its key role in P-cluster maturation, $NifH_2$ is also required for FeMo-co insertion into $NifD_2K_2$.[19,20] Thereby, $^{\Delta H}NifD_2K_2$§ contains immature P-clusters, but no FeMo-co. Previous work from our laboratories has demonstrated that $^{\Delta H}NifD_2K_2$ accumulates as a variety of $NifD_2K_2$ species, including those having no accessory proteins attached and those bound to either NafH, NifW or NifZ.[13] Although the specific functions of these factors are not yet known, biochemical experiments have indicated they sequentially and differentially interact with $NifD_2K_2$ during P-cluster maturation in the order NafH, NifW, NifZ. Prior work has also established that, to date, there is no biochemical or physiological defect associated with loss of NafH function,[21] whereas inactivation of NifW results in slower diazotrophic growth due to low accumulation of active $NifD_2K_2$.[22] Inactivation of NifZ also entails slower diazotrophic growth resulting from the accumulation of a mixed population of $NifD_2K_2$ species including both fully mature $NifD_2K_2$ and a variety of inactive or partially active species.[14,21] Among those, some are bound to NifW. These observations have led to the suggestion that NifW serves to stabilize a form of immature $NifD_2K_2$ at an early stage in P-cluster maturation and that NifZ could be involved in the dissociation of NifW and further recruitment of $NifH_2$ in the final stage of P-cluster maturation. In the present work, the biophysical properties of cluster species contained in both immature $NifD_2K_2$ having no bound accessory protein and immature $NifD_2K_2$ with two associated NifW were examined by electron paramagnetic resonance (EPR) and X-ray absorption (XAS) spectroscopies.

Results

Mature P-clusters in resting state $NifD_2K_2$ are diamagnetic and therefore do not exhibit any EPR signature, whereas FeMo-co is paramagnetic and exhibits a characteristic $S = 3/2$ EPR signal.[2] Thus, reduced, fully matured $NifD_2K_2$ shows an EPR signature associated with the presence of FeMo-co only. In contrast, $^{\Delta H}NifD_2K_2$ lacks the $S = 3/2$ EPR signature associated with FeMo-co but exhibits a complex $S = 1/2$ signature that has been assigned as a precursor to mature P-cluster formation.[16,23] Comparison of EPR analysis of $^{\Delta Z}NifD_2K_2$ or $^{\Delta H}NifD_2K_2$ suggested that the complex $S = 1/2$ signature associated with immature P-clusters corresponds to two electronic isomers having close g-tensors of [2.06, 1.93, 1.89] and [2.03, 1.93, 1.86].[13,14] Furthermore, fractionation of affinity-purified $^{\Delta Z}NifD_2K_2$ could be resolved into populations that include $^{\Delta Z}NifD_2K_2$ with no associated accessory protein, $^{\Delta Z}NifD_2K_2$ with one NifW bound ($^{\Delta Z}NifD_2K_2W$), and $^{\Delta Z}NifD_2K_2$ with two bound NifW ($^{\Delta Z}NifD_2K_2W_2$).[14] Initial EPR studies of isolated $^{\Delta Z}NifD_2K_2W_2$ revealed a single $S = 1/2$ species with $g = [2.02, 1.93, 1.86]$. Nevertheless, analysis of the $^{\Delta Z}NifD_2K_2$ fraction for which no NifW is bound is complicated since inactivation of NifZ does not directly affect FeMo-co formation and only slows, but does not eliminate, P-cluster maturation.[14]

To allow the isolation of a highly enriched fraction of $^{\Delta Z}NifD_2K_2$ containing immature P-clusters and lacking both FeMo-co and bound NifW, a strain was constructed in which both the *nifH* and *nifZ* genes are deleted. The Strep-tag placed at the N-terminus of NifD in this construct enables affinity purification of $^{\Delta H\Delta Z}NifD_2K_2$ fractions that are highly enriched for species uniformly deficient in FeMo-co assembly and P-cluster maturation. $^{\Delta H\Delta Z}NifD_2K_2$ was further fractionated using anion exchange chromatography allowing isolation of fractions corresponding to $^{\Delta H\Delta Z}NifD_2K_2$ (no NifW attached to $NifD_2K_2$) and $^{\Delta H\Delta Z}NifD_2K_2W_2$ (two NifW attached) (Fig. 2, S1 and S2†).

The availability of separable forms of $NifD_2K_2$ harboring immature P-clusters and having no associated FeMo-co, with or without NifW bound, permitted the detailed biophysical comparison of these species. UV-vis measurements of the isolated samples showed slight differences in their spectra, suggesting subtle structural changes upon binding of NifW

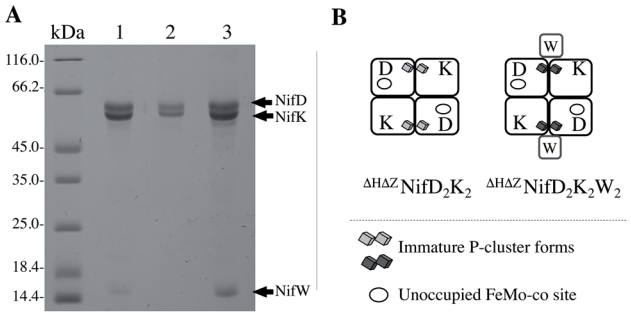

Fig. 2 $NifD_2K_2$ species characterized in this work. (A) SDS-PAGE analysis of proteins isolated by one-step Strep-tag affinity purification (1), and $^{\Delta H\Delta Z}NifD_2K_2$ (2) and $^{\Delta H\Delta Z}NifD_2K_2W_2$ (3) isolated by ion-exchange chromatography of the sample shown in (1). Molecular weight standards are shown on the left lane. The presence of a small amount of a $^{\Delta H\Delta Z}NifD_2K_2NafH_X$ species (less than 8% of the total sample) in (3) was revealed by SDS-PAGE analysis of more concentrated samples as shown in Fig. S1.† (B) Schematic representation of samples shown in (A). Interaction of NifW at the interface of $NifD_2K_2$ is only shown for convenience and has not been experimentally established. Corresponding X-band EPR spectra are provided in Fig. S2.†

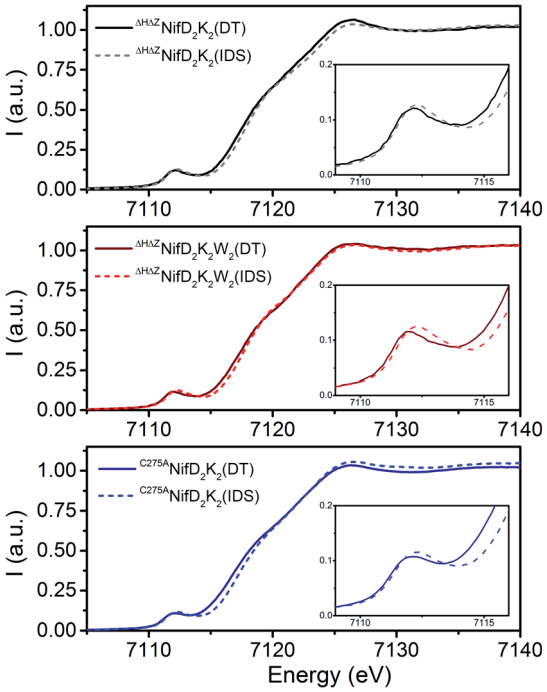

Fig. 3 Comparison of the normalized Fe K-edge XAS spectra of $^{\Delta H\Delta Z}NifD_2K_2$ (top), $^{\Delta H\Delta Z}NifD_2K_2W_2$ (middle), and $^{C275A}NifD_2K_2$ (bottom) in the DT-reduced (solid) and IDS-oxidized (dashed) forms. Insets show an expanded view of the pre-edge region from 7109–7116 eV.

(Fig. S3†). To characterize the structural and spectroscopic properties of these clusters, XAS and EPR spectroscopic analyses were performed. For comparative purposes, apo-$NifD_2K_2$ was also purified and characterized from a strain in which the FeMo-cofactor anchoring 275Cys residue is substituted by 275Ala (abbreviated as $^{C275A}NifD_2K_2$). $^{C275A}NifD_2K_2$ contains mature P-clusters, but no FeMo-co.[13]

To determine the influence of NifW on immature P-cluster oxidation state and geometry, X-ray absorption spectroscopy (XAS) at the Fe K-edge was performed for $^{\Delta H\Delta Z}NifD_2K_2$, $^{\Delta H\Delta Z}NifD_2K_2W_2$, and $^{C275A}NifD_2K_2$ in both the dithionite (DT)-reduced and indigo disulfonate (IDS)-oxidized states.

As previously noted, $^{C275A}NifD_2K_2$ does not contain FeMo-co but contains mature P-clusters, thus providing a useful internal control for comparison of immature and mature P-cluster species.[13] Fig. 3 compares the DT-reduced and IDS-oxidized forms of each variant under investigation. All spectra appear typical for [Fe:S] clusters, with a single well-defined pre-edge feature ~7112 eV leading into an edge presenting a shoulder at ~7118 eV.[17,24–27] Upon oxidation, all variants exhibit an increase in both intensity and energetic position of the pre-edge feature, as well as an increase in the energetic position of the rising edge (7115–7119 eV). The position of the pre-edge and rising edge can serve as diagnostics of oxidation state, shifting to higher energies with increased oxidation state. Meanwhile, pre-edge intensity at the Fe K-edge derives from both lowering of centrosymmetry, which induces Fe 3d–4p mixing, and the number of available holes in the valence shell of Fe.[28,29] Hence, relative increases in pre-edge intensity can arise from either a decrease in local symmetry, increase in oxidation state, or some combination. Therefore, these changes are all consistent with some degree of Fe-centered oxidation upon exposure to IDS. The observed shift in the rising edge moving from $^{C275A}NifD_2K_2(DT)$ → $^{C275A}NifD_2K_2(IDS)$ is +0.7 eV. Previous studies have already established that exposure to IDS oxidizes the mature, all-ferrous P-cluster (P^N) to a two-electron oxidized form (P^{2+}).[30] Therefore, this +0.7 eV increase in the rising edge can be used as a tentative diagnostic for two-electron oxidation. This is consistent with previous observations for the DT-reduced and IDS-oxidized forms of $^{\Delta B}NifD_2K_2$, which, like $^{C275A}NifD_2K_2$, contains mature P-clusters but no FeMo-co, and displayed a relative shift of +0.6 eV.[17] Meanwhile, the observed shifts in the rising edge for both $^{\Delta H\Delta Z}NifD_2K_2(DT)$ → $^{\Delta H\Delta Z}NifD_2K_2(IDS)$ and $^{\Delta H\Delta Z}NifD_2K_2W_2(DT)$ → $^{\Delta H\Delta Z}NifD_2K_2W_2(IDS)$ are +0.35 eV, half that found for $^{C275A}NifD_2K_2$. Therefore, exposure of either immature P-cluster variant to IDS likely results in a one-electron oxidation event.

Comparison of the DT-reduced forms of the three variants reveals that $^{\Delta H\Delta Z}NifD_2K_2(DT)$ and $^{\Delta H\Delta Z}NifD_2K_2W_2(DT)$ display a nearly superimposable rising edge between 7114–7118 eV, shifted by +0.7 eV relative to $^{C275A}NifD_2K_2(DT)$ (Fig. S4†). This shift is approximately the same as observed when $^{C275A}NifD_2K_2(DT)$ and $^{C275A}NifD_2K_2(IDS)$ (Fig. 3) are compared, supporting an interpretation that $^{\Delta H\Delta Z}NifD_2K_2(DT)$ and $^{\Delta H\Delta Z}NifD_2K_2W_2(DT)$ are both two-electron oxidized relative to $^{C275A}NifD_2K_2(DT)$. Similarly, the rising edges of the IDS-oxidized forms of $^{\Delta H\Delta Z}NifD_2K_2$ and $^{\Delta H\Delta Z}NifD_2K_2W_2$ are nearly superimposable and shifted by +0.35 eV relative to $^{C275A}NifD_2K_2(IDS)$. Interestingly, while the Fe K-edge spectra of $^{\Delta H\Delta Z}NifD_2K_2(IDS)$ and $^{\Delta H\Delta Z}NifD_2K_2W_2(IDS)$ are extremely similar, the DT-reduced forms exhibit significant deviations at the pre-edge, around 7112 eV. Namely, while the pre-edge intensities of both $^{\Delta H\Delta Z}NifD_2K_2(DT)$ and $^{\Delta H\Delta Z}NifD_2K_2W_2(DT)$ are more intense than $^{C275A}NifD_2K_2(DT)$, $^{\Delta H\Delta Z}NifD_2K_2W_2(DT)$ appears shifted to

lower energy by −100 meV relative to either $^{\Delta H\Delta Z}$NifD$_2$K$_2$(DT) or ^{C275A}NifD$_2$K$_2$(DT). Besides oxidation state, local symmetry and coordination environment can play a role in energetic position and intensity distribution of the pre-edge, and this shift may be indicative of local structural differences in the Fe environments of $^{\Delta H\Delta Z}$NifD$_2$K$_2$(DT) and $^{\Delta H\Delta Z}$NifD$_2$K$_2$W$_2$(DT). Based on these results proposed Fe oxidation state distributions of the three variants are summarized in Table 1. These distributions are assigned assuming 8 unique Fe per NifDK unit.

The direct overlay of the Fe K-edge XAS spectra of $^{\Delta H\Delta Z}$NifD$_2$K$_2$(DT), $^{\Delta H\Delta Z}$NifD$_2$K$_2$W$_2$(DT), and ^{C275A}NifD$_2$K$_2$(IDS) further supports these oxidation state distribution assignments, where the rising edges (7115–7119 eV) of these three samples are superimposable (Fig. S5†). Overlays of the pre-edge regions additionally support small variations in local geometry.

To obtain further information on these species, Fe K-edge EXAFS measurements were performed (Fig. 4 and S6–S8†). As shown in Fig. 4, all spectra exhibit either one or two dominant features around 1.9 and 2.4 Å, which may be attributed to Fe–S and Fe–Fe scatterers, respectively. In ^{C275A}NifD$_2$K$_2$(DT), only the dominant Fe–S scatterer is observed due to near complete phase cancellation of the two distinct Fe–Fe scattering paths, Fe–Fe(1) and Fe–Fe(2). This has been previously observed in studies of both mature NifD$_2$K$_2$ and $^{\Delta B}$NifD$_2$K$_2$.[17,24,25,31] However, this is not the case for either $^{\Delta H\Delta Z}$NifD$_2$K$_2$(DT) or $^{\Delta H\Delta Z}$NifD$_2$K$_2$W$_2$(DT) which display clear features at 2.4 Å, similar to previous observations for [4Fe:4S] cubane clusters and $^{\Delta H}$NifD$_2$K$_2$.[17,25,26] In the IDS-oxidized form of ^{C275A}NifD$_2$K$_2$ this feature is apparent, although at a significantly lower intensity in the FTs (Fig. 4 and S6†). This is likely due to the significant structural changes that have been crystallographically observed to accompany the oxidation of mature P-cluster, including light atom coordination of Fe and partial Fe–S bond dissociation.[15,32] In the P^{2+} state, one of the two sub-cubanes assumes an open conformation, with two iron atoms (Fe_5 and Fe_6) partially dissociated from the bridging sulfide to ligate the backbone amide of a cysteine and the hydroxyl group of a serine, respectively (Fig. 1). A considerable number of other differences are also observed among all three variants for ∼1.9 and ∼2.4 Å scattering features, including variations in total intensity, relative intensity, and small variations in radial distribution. These imply all three variants exhibit structures that are distinct from one another. However, as these spectra involve the complex overlap of at least 3–4 scattering paths, direct interpretation of the absolute values of the *R*-space spectra are non-diagnostic.

To gain physical insight into these changes, a minimalist model was used to fit the data, involving a single Fe–S scattering path and two unique Fe–Fe scattering paths. The use of two unique Fe–Fe scattering paths is necessitated due to the wide distribution of Fe–Fe distances observed in the mature P-cluster as well as in iron–sulfur cubane clusters.[24,33] In addition, the presence of O and N coordination of Fe observed in crystal structures of oxidized mature P-cluster prompted us to test whether such coordination environments exist in the immature variants, using fits that included light atom scatterers.[15,32] The resulting best fit parameters for models both with and without an Fe–O scatterer are provided in Table S1.† It is important to note that while an Fe–O scatterer was employed in these models, the similar electron density of O and N make them virtually indistinguishable from one another, and therefore this scattering pathway represents a sum of both possible Fe–O and Fe–N coordination.

Due to the high degree of correlation between scattering path degeneracy, *N*, and bond variance, σ^2, it is generally difficult to accurately fit both simultaneously without some structural reference to restrict *N*. To fit the unknown structures of the clusters in $^{\Delta H\Delta Z}$NifD$_2$K$_2$ and $^{\Delta H\Delta Z}$NifD$_2$K$_2$W$_2$, the sum of *N* for Fe–Fe(1) and Fe–Fe(2) was fixed to 3, which is the theoretical Fe–Fe path degeneracy for a [4Fe:4S] cubane cluster, and the ratios of *N* for either path were allowed to vary. As there are 8 unique Fe absorbers in each variant, the minimal increment in *N* for Fe–O/N and Fe–S scattering paths was limited to 0.125. Meanwhile, the minimal increment used in variation of the Fe–Fe

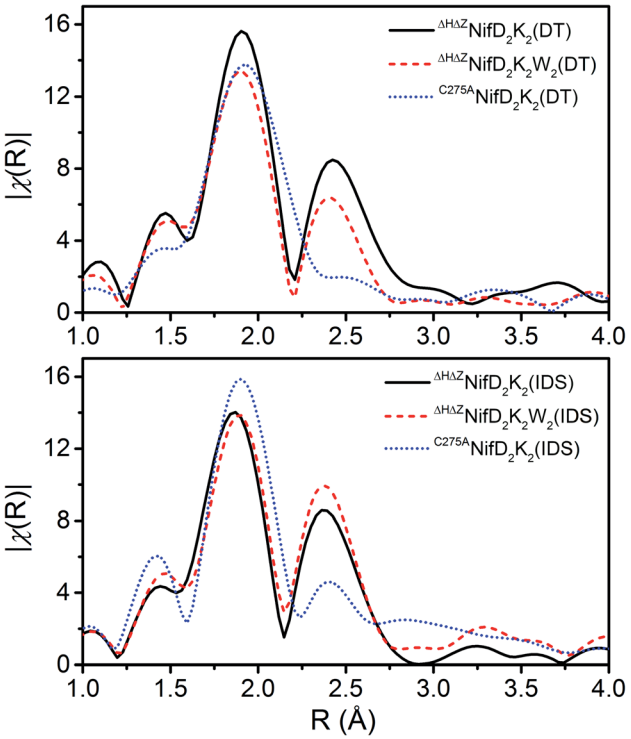

Fig. 4 Comparisons of the Fourier transforms (FTs) of the Fe K-edge EXAFS of the DT-reduced and IDS-oxidized forms of $^{\Delta H\Delta Z}$NifD$_2$K$_2$ (black), $^{\Delta H\Delta Z}$NifD$_2$K$_2$W$_2$ (red), and ^{C275A}NifD$_2$K$_2$ (blue) in *R*-space. Spectra are k^3-weighted, and FTs were performed for a *k*-range of 3–13 Å. No phase-shift was applied.

Table 1 Summary of proposed Fe oxidation state distributions of the cluster species found in $^{\Delta H\Delta Z}$NifD$_2$K$_2$ and $^{\Delta H\Delta Z}$NifD$_2$K$_2$W$_2$, based on Fe K-edge XAS

Sample	DT-reduced	IDS-oxidized
$^{\Delta H\Delta Z}$NifD$_2$K$_2$	[6Fe^{II}2Fe^{III}]	[5Fe^{II}3Fe^{III}]
$^{\Delta H\Delta Z}$NifD$_2$K$_2$W$_2$	[6Fe^{II}2Fe^{III}]	[5Fe^{II}3Fe^{III}]
^{C275A}NifD$_2$K$_2$	[8Fe^{II}]	[6Fe^{II}2Fe^{III}]

scattering paths was 0.25, as the loss or addition of a single Fe–Fe scatterer must be observed by both Fe involved. The degeneracies of each pathway for ^{C275A}NifD$_2$K$_2$(DT) and ^{C275A}NifD$_2$K$_2$(IDS) were determined from equivalent crystal structures of the mature P-cluster in the P^N and the P^{2+} states and fixed during fitting.[15,33]

As shown in Table S1,† the fit Fe–S, Fe–Fe(1), and Fe–Fe(2) scattering distances all appear to fall within typical ranges for both varying forms of the P-cluster and more generally for homometallic iron–sulfur clusters.[34–38] A comparison of the fit parameters of the respective DT-reduced and IDS-oxidized forms reveals only relatively minor contractions for $^{\Delta H\Delta Z}$NifD$_2$K$_2$ and $^{\Delta H\Delta Z}$NifD$_2$K$_2$W$_2$. These changes are considerably more significant when comparing ^{C275A}NifD$_2$K$_2$(DT) and ^{C275A}NifD$_2$K$_2$(IDS), which exhibit contractions of ~0.06 Å and ~0.10 Å in Fe–Fe(1) and Fe–Fe(2), respectively. However, based on the Fe oxidation state distributions for the DT-reduced and IDS-oxidized variants, these larger contractions are not surprising due to ^{C275A}NifD$_2$K$_2$(IDS) being two-electron oxidized relative to ^{C275A}NifD$_2$K$_2$(DT). Notably, the structural parameters of $^{\Delta H\Delta Z}$NifD$_2$K$_2$(DT), $^{\Delta H\Delta Z}$NifD$_2$K$_2$W$_2$(DT), and ^{C275A}NifD$_2$K$_2$(IDS) appear quite similar, further supporting the oxidation state distribution assignments shown in Table 1 (Fig. S8†).

Inclusion of an Fe–O/N scattering pathway provides an improved fit for all variants in both DT-reduced and IDS-oxidized forms in terms of χ^2 and *R*-factors. This is not unexpected, as increasing the number of free parameters in a model will typically provide a better fit in terms of mean square deviation. However, fits performed for $^{\Delta H\Delta Z}$NifD$_2$K$_2$W$_2$ involving an Fe–O scatterer show significantly greater improvement in these parameters than for either $^{\Delta H\Delta Z}$NifD$_2$K$_2$ or ^{C275A}NifD$_2$K$_2$. This is also clearly visualized in Fig. 5, where the inclusion of the Fe–O scattering contribution to the fit provides only a slight improvement between 1.25–1.75 Å for $^{\Delta H\Delta Z}$NifD$_2$K$_2$(DT), but a significant improvement over this same *R*-range for ^{C275A}NifD$_2$K$_2$(DT).

To evidence the statistical improvement gained in fits of $^{\Delta H\Delta Z}$NifD$_2$K$_2$W$_2$ by inclusion of an Fe–O scattering path, we have included the reduced χ^2 statistic in Table S1.† This parameter is calculated by dividing the root mean-square deviation, χ^2, by the difference between the total number of degrees of freedom and the free parameters used in the fit. The number of degrees of freedom (χ_{ind}) is calculated by eqn (1).

$$\chi_{ind} = \frac{2(k_{max} - k_{min})(R_{max} - R_{min})}{\pi} \quad (1)$$

For the present spectra χ_{ind} equates to 12.4. When including an Fe–O scattering path to the EXAFS model, two additional free parameters are necessary, raising the total number of free parameters from 7 to 9 while the total number of degrees of freedom remains the same. This reduces the unused number of degrees of freedom from 5.4 to 3.4, meaning a >1.6-fold improvement in χ^2 must be achieved to improve the reduced χ^2 statistic. Given the weak scattering properties of O compared to heavier atoms such as S and Fe, the presence of an Fe–O scatterer is not expected to make particularly large spectral

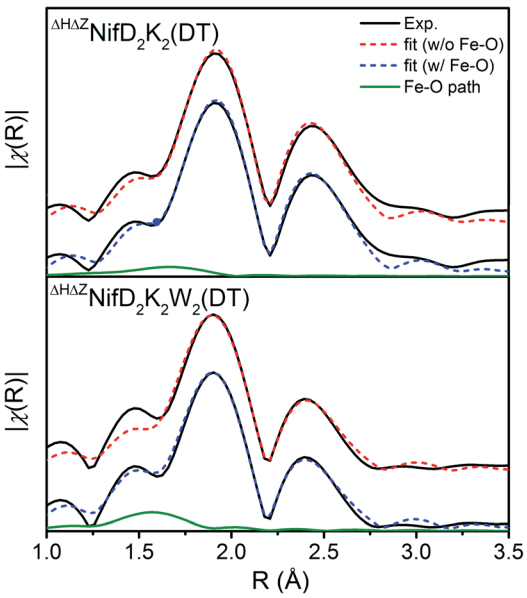

Fig. 5 Comparison of the Fe K-edge EXAFS of DT-reduced $^{\Delta H\Delta Z}$NifD$_2$K$_2$ (top) and $^{\Delta H\Delta Z}$NifD$_2$K$_2$W$_2$ (bottom) experimental spectra (black) and respective best fit models with (blue, dashed) and without (red, dashed) inclusion of an Fe–O/N scattering path contribution (green, solid). Corresponding fit parameters are provided in Table S1.† Spectra are k^3-weighted, and FTs were performed for a *k*-range of 3–13 Å. Fits were performed using k^3-weighting over ranges of k = 3–13 Å^{-1} and R = 1–3 Å.

contributions. In turn, reduced χ^2 serves as a particularly harsh measure of statistical significance. Nevertheless, the reduced χ^2 statistic is improved for both $^{\Delta H\Delta Z}$NifD$_2$K$_2$W$_2$(DT) and $^{\Delta H\Delta Z}$NifD$_2$K$_2$W$_2$(IDS) by inclusion of an Fe–O scatterer with N = 0.5. These statistical improvements are nearly invariant for a range of 0.25–0.5, equating to the coordination of 2–4 light atoms (O or N) per immature P-cluster of $^{\Delta H\Delta Z}$NifD$_2$K$_2$W$_2$.

While the presence of Fe–O/N coordination in $^{\Delta H\Delta Z}$NifD$_2$K$_2$W$_2$ is well supported by the observed statistical improvements, inclusion of this scattering path to fits of either $^{\Delta H\Delta Z}$NifD$_2$K$_2$ or ^{C275A}NifD$_2$K$_2$ results in a poorer reduced χ^2 statistic, with increases of 40–80%. However, this lack of improvement in reduced χ^2 does not exclude the possibility that light atom scatterers are present in the Fe coordination environments of these samples. Namely, the overall contribution of such a light atom scatterer to the EXAFS is expected to be small, especially considering that heavier scatterers such as S and Fe are present. Additionally, variation in bond distances between Fe and O or N can greatly affect whether these scattering paths will accumulate into some significant spectral contribution. For example, the P^{2+} state of the mature P-cluster displays Fe–O coordination from the NifK ^{Ser}188 residue at 1.90 Å, and Fe–N from the NifD ^{Cys}88 residue at 2.15 Å.[15]

Due to the large difference in distances of these two bonds (0.25 Å), attempts to account for both with a single scattering path would require a very large bond variance σ^2, which would further diminish the contributions of these already weak scattering paths to the total EXAFS spectrum. With such small

contributions it is little surprise that inclusion of an Fe–O/N scatterer to ^{C275A}NifD$_2$K$_2$(IDS), which contains mature P^{2+}, does not significantly improve reduced χ^2.

The oxidation state assignments from our XAS studies (Table 1) imply that the IDS-oxidized forms of $^{\Delta H\Delta Z}$NifD$_2$K$_2$ and $^{\Delta H\Delta Z}$NifD$_2$K$_2$W$_2$ should be paramagnetic, and possibly the DT-reduced forms as well. Therefore, to further investigate the electronic structures of $^{\Delta H\Delta Z}$NifD$_2$K$_2$ and $^{\Delta H\Delta Z}$NifD$_2$K$_2$W$_2$, X-band EPR measurements of these systems were performed. The EPR spectra of DT-reduced $^{\Delta H\Delta Z}$NifD$_2$K$_2$ and $^{\Delta H\Delta Z}$NifD$_2$K$_2$-W$_2$ (Fig. 6 and S2†) are dominated by broad $S = 1/2$ signals similar to those previously observed in $^{\Delta Z}$NifD$_2$K$_2$.[14] $^{\Delta H\Delta Z}$NifD$_2$K$_2$ displays a slightly rhombically distorted axial signal, with clear inflections at $g \approx 2.05$, 1.93, and 1.90. Meanwhile, $^{\Delta H\Delta Z}$NifD$_2$K$_2$W$_2$ is dominated by an axial signal with inflections at $g \approx 2.04$ and 1.93, and additional shoulders appearing at $g \approx 2.07$ and 1.88. Additionally, both $^{\Delta H\Delta Z}$NifD$_2$K$_2$ and $^{\Delta H\Delta Z}$NifD$_2$K$_2$W$_2$ samples exhibit weak signals at $g \approx 5.60$ and 5.11, consistent with transitions anticipated for an $S = 3/2$ system with negative zero-field splitting. These signals had previously been detected in $^{\Delta H}$NifD$_2$K$_2$ and $^{\Delta Z}$NifD$_2$K$_2$, but are not present in $^{\Delta B}$NifD$_2$K$_2$, implying they are associated with an immature P-cluster species.[14] The appearance of a very minor signal $g \approx 7.3$ is also observed in $^{\Delta H\Delta Z}$NifD$_2$K$_2$, possibly corresponding to the $M_S = \pm 1/2$ manifold of an $S = 5/2$ signal. SDS-PAGE analysis of the $^{\Delta H\Delta Z}$NifD$_2$K$_2$W$_2$ sample (Fig. S1†) reveals the presence of a low amount of NafH, which could suggest that elements of the spectrum might originate from a low level of NifD$_2$K$_2$ with bound NafH. However, the normalized intensities of this signal are invariant between the protein isolated by one-step Strep-tag affinity purification and the further-purified $^{\Delta H\Delta Z}$NifD$_2$K$_2$ and $^{\Delta H\Delta Z}$NifD$_2$K$_2$W$_2$ fractions, supporting that this signal is independent of NafH (Fig. S2†). Alternatively, a similar $S = 3/2$ signal has also been observed in the X-band EPR spectrum of NifH$_2$, which contains a subunit-bridging [4Fe:4S] cluster, as well as other [Fe:S] clusters having dominant $S = 1/2$ signals.[39–42] The $S = 3/2$ signal observed here therefore may belong to an $S = 1/2$, 3/2 spin admixture, originating from a cluster species with an exchange-coupled system.[43,44]

Variable temperature measurements were performed to further characterize and quantify the observed EPR signals (Fig. 6). The obtained spectra reveal similar saturation behavior in DT-reduced $^{\Delta H\Delta Z}$NifD$_2$K$_2$ and $^{\Delta H\Delta Z}$NifD$_2$K$_2$W$_2$, with saturation observed below 12 K and temperature dependent broadening occurring above 20 K. This narrow temperature range of unsaturated signal intensity has been commonly observed in $S = 1/2$ $[4Fe:4S]^+$ clusters.[45] Meanwhile, the temperature-corrected intensities of the respective $S = 3/2$ signals are relatively invariant across the measured temperature range. Based on the Asaa–Vanngard corrected spin-integration against a $CuSO_4$ standard, the $S = 1/2$ signal of DT-reduced samples accounts for ~3.75 spins/$^{\Delta H\Delta Z}$NifD$_2$K$_2$ and ~3.5 spins/$^{\Delta H\Delta Z}$NifD$_2$K$_2$W$_2$, respectively.[46] By comparison, the minor $S = 3/2$ signal accounts for approximately 0.3 spins in either DT-reduced $^{\Delta H\Delta Z}$NifD$_2$K$_2$ or $^{\Delta H\Delta Z}$NifD$_2$K$_2$W$_2$; we note the broadness of this signal precludes precise quantification. These results support ~2 spins per NifDK(W) unit, indicating the spectra presented in Fig. 6 represent a convolution of at least two unique $S = 1/2$ species having similar spectral properties. When combined with the described XAS measurements, these results support the presence of two unique $[4Fe:4S]^+$ clusters in both $^{\Delta H\Delta Z}$NifD$_2$K$_2$ and $^{\Delta H\Delta Z}$NifD$_2$K$_2$W$_2$.

In the context of the P-cluster, the potential presence of two unique $[4Fe:4S]^+$ per NifDK unit of $^{\Delta H\Delta Z}$NifD$_2$K$_2$ and $^{\Delta H\Delta Z}$NifD$_2$K$_2$W$_2$ is not surprising. However, if these clusters were in relatively close spatial proximity, as would be required for formation of the mature P-cluster, some significant degree of spin–spin coupling would be anticipated.[47] Additionally, simulations of $^{\Delta H\Delta Z}$NifD$_2$K$_2$(DT) or $^{\Delta H\Delta Z}$NifD$_2$K$_2$W$_2$(DT) using either a single $S = 1/2$ component or two uncoupled $S = 1/2$ components in a 1 : 1 stoichiometry cannot reasonably account for either the level of broadening or additional inflections around $g = 2$ observed in these spectra. Therefore, to investigate these species further, parallel mode X-band measurements of DT-reduced $^{\Delta H\Delta Z}$NifD$_2$K$_2$ and $^{\Delta H\Delta Z}$NifD$_2$K$_2$-W$_2$ were performed (Fig. 7).

The transition selection rule for parallel mode detection is $\Delta m_S = 0$, and thus requires mixing of m_S levels to gain intensity. Such mixing occurs in a limited number of circumstances. Examples include (i) Kramer's systems with half-integer $S > \frac{1}{2}$ and very weak zero-field splitting (on the order of the Zeeman effect), (ii) non-Kramer's systems with energetically close lying

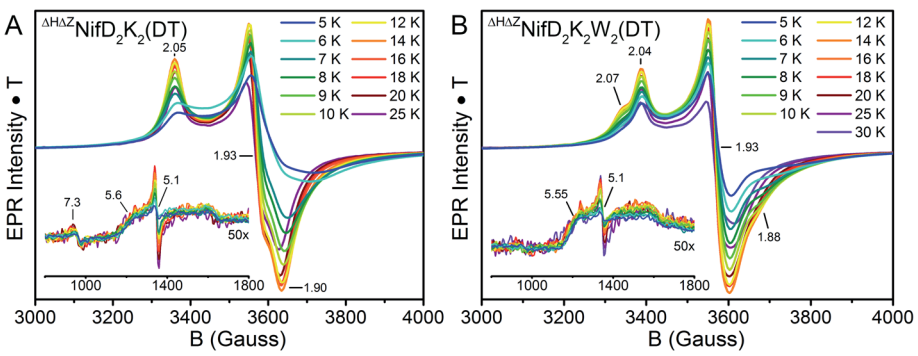

Fig. 6 Temperature-dependent X-band EPR of DT-reduced (A) $^{\Delta H\Delta Z}$NifD$_2$K$_2$ and (B) $^{\Delta H\Delta Z}$NifD$_2$K$_2$W$_2$. Spectra were collected using 1 mW power at 9.65 GHz. All spectra are normalized for power, gain, collection time, and temperature.

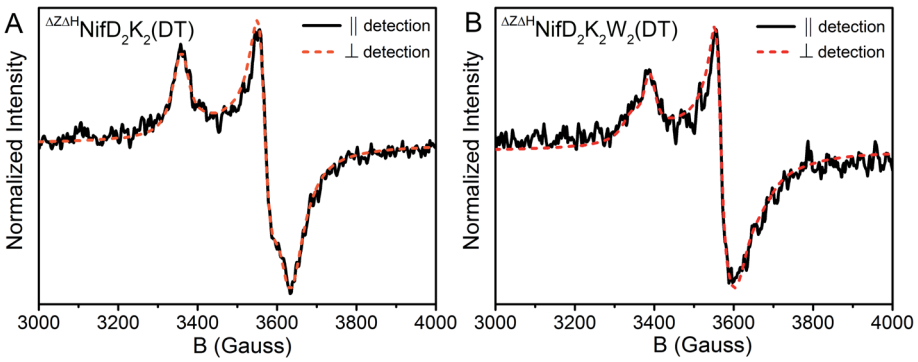

Fig. 7 Comparison of perpendicular (black, solid) and parallel mode (red, dashed) X-band EPR spectra of DT-reduced (A) $^{\Delta H\Delta Z}$NifD$_2$K$_2$ and (B) $^{\Delta H\Delta Z}$NifD$_2$K$_2$W$_2$. Spectra were measured at 16 K, 1 mW, and 9.65 GHz.

integer spin levels, and (iii) spin-coupled systems in which the coupling strength competes with the Zeeman effect.[48] Parallel mode intensity is observed in spectra of both DT-reduced $^{\Delta H\Delta Z}$NifD$_2$K$_2$ and $^{\Delta H\Delta Z}$NifD$_2$K$_2$W$_2$, indicating the observed signals could originate from weak spin-coupling. On this basis, spectra of $^{\Delta H\Delta Z}$NifD$_2$K$_2$ and $^{\Delta H\Delta Z}$NifD$_2$K$_2$W$_2$ were each fit using two spin-coupled $S = 1/2$ systems (Fig. S9 and Table S2†). Due to the large number of parameters involved in fitting such a system, a definitive, unique fit was not possible. Spectra of $^{\Delta H\Delta Z}$NifD$_2$K$_2$ could be reasonably fit using two overlapping $S = 1/2$ systems with equal contributions in the absence of spin-coupling. Inclusion of spin-coupling resulted in an estimate of $J = 1.2 \times 10^{-3}$ cm^{-1} between two $M_S = 1/2$ components *a* and *b* with $g_a = [2.06, 1.91, 1.91]$ and $g_b = [2.05, 1.93, 1.86]$, corresponding to a lower limit on the e^-–e^- distance of approximately 11 Å based on the point-dipole approximation. Meanwhile, spectra of $^{\Delta H\Delta Z}$NifD$_2$K$_2$W$_2$ required the use of spin coupling to be simulated, with a larger axial e^-–e^- coupling of $J = 3.3 \times 10^{-3}$ cm^{-1} between $g_a = [2.05, 1.93, 1.90]$ and $g_b = [2.06, 1.93, 1.87]$, resulting in a reduced e^-–e^- distance of ~8 Å. The dependence of the simulated spectra on the magnitude of the principal values of the e^-–e^- coupling interaction matrix is provided in Fig. S10.† Although the point-dipole approximation has been shown to overestimate e^-–e^- distances in spin-delocalized systems, the relative inter-cluster distances are expected to remain consistent given the similarity of $^{\Delta H\Delta Z}$NifD$_2$K$_2$(DT) and $^{\Delta H\Delta Z}$NifD$_2$K$_2$W$_2$(DT). These results support that $^{\Delta H\Delta Z}$NifD$_2$K$_2$(DT) and $^{\Delta H\Delta Z}$NifD$_2$K$_2$W$_2$(DT) consist of two unique, separate $[4Fe:4S]^+$ clusters, and that the distance between these clusters is decreased in the NifW-bound form.

Further EPR measurements were performed on IDS-oxidized samples. Mature P-cluster in the P^{2+} state exhibits a low-field parallel mode signal (appearing at $g \approx 12.0$ for *A. vinelandii* NifD$_2$K$_2$, $g = 15.6$ for *Xanthobacter autotrophicus* NifD$_2$K$_2$, and $g = 16.0$ for *Gluconacetobacter diazotrophicus* NifD$_2$K$_2$) associated with an integer spin system.[48,49] This is not the case for IDS-oxidized $^{\Delta H\Delta Z}$NifD$_2$K$_2$ or $^{\Delta H\Delta Z}$NifD$_2$K$_2$W$_2$, in agreement with previous reports for $^{\Delta H}$NifD$_2$K$_2$.[16] Given the EPR features observed for $^{\Delta H\Delta Z}$NifD$_2$K$_2$(DT) and $^{\Delta H\Delta Z}$NifD$_2$K$_2$W$_2$(DT) combined with the XAS-based oxidation state assignments summarized in Table 1, IDS-oxidized samples of both species were anticipated to be non-integer spin. Indeed, IDS oxidation of either $^{\Delta H\Delta Z}$NifD$_2$K$_2$ or $^{\Delta H\Delta Z}$NifD$_2$K$_2$W$_2$ resulted in the complete disappearance of the spectra observed for the dithionite-reduced species, and the appearance of a new, complicated set of signals in the CW X-band EPR (Fig. 8). Importantly, re-reduction of these samples with sodium dithionite after desalting resulted in spectra identical to the reduced states presented in Fig. 6 (see Fig. S11†). Therefore, IDS-oxidation of $^{\Delta H\Delta Z}$NifD$_2$K$_2$ and $^{\Delta H\Delta Z}$NifD$_2$K$_2$W$_2$ is a reversible process, and none of the features observed in these spectra appear to originate from cluster damage.

In the IDS-oxidized forms of both $^{\Delta H\Delta Z}$NifD$_2$K$_2$ and $^{\Delta H\Delta Z}$NifD$_2$K$_2$W$_2$, low-field inflections are clearly observed starting at $g = 5.8$ and 4.3 (Fig. 8, insets). Temperature-dependent measurements reveal an increase in intensity of the $g = 4.3$ inflection between 5–20 K, followed by a decrease in intensity above 20 K. This result is consistent with the presence of a rhombic $S = 5/2$ species, with the $g = 4.3$ inflection arising from population of the $M_s = 3/2$ manifold as a function of temperature. Meanwhile, the presence of an inflection at $g = 5.8$ at low temperatures is consistent with the presence of an $S = 3/2$ species with negative zero-field splitting, like that observed in the equivalent DT-reduced species (Fig. S12†).

At intermediate fields (3200-3800 G), the spectra of IDS-oxidized $^{\Delta H\Delta Z}$NifD$_2$K$_2$ and $^{\Delta H\Delta Z}$NifD$_2$K$_2$W$_2$ become complex and strongly temperature dependent. At low temperatures both display inflections at g ~2.00 (sharp) and 1.94 (broad). The extremely broad nature of the signal centered around 1.94 is consistent with rapid spin-lattice relaxation. At temperatures above 20 K, this broad signal quickly disappears and is replaced by a well-defined axial $S = 1/2$ signal having inflections at $g = 2.00$, 2.00 and 1.94, which take full form at 40 K ($^{\Delta H\Delta Z}$NifD$_2$K$_2$) and 45 K ($^{\Delta H\Delta Z}$NifD$_2$K$_2$W$_2$). These signals continue to persist at higher temperatures without any significant decrease in intensity, similar to previous observations for [2Fe:2S] and [3Fe:4S] clusters.[45,50] Additionally, both species display further minor inflections at $g = 2.05$, 1.92 and 1.86, and possibly at 2.15 and 2.09 as well. A similarly shaped $S = 1/2$ spectrum has been observed for the minor component of the OX state of the open-cubane active site of the hybrid cluster protein (Hcp), but differs significantly in both temperature dependence and observed *g*-

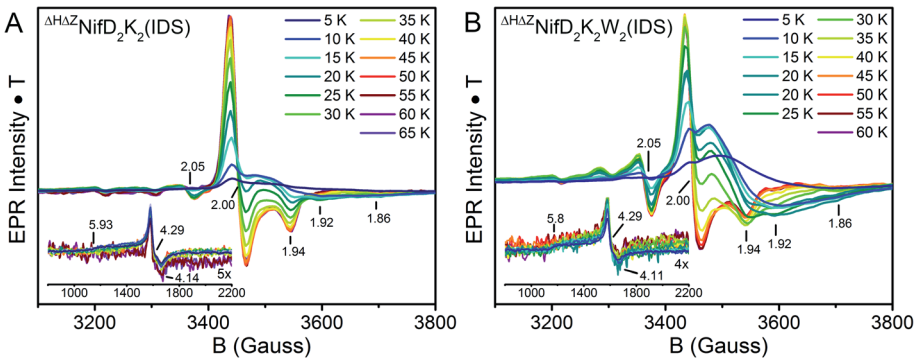

Fig. 8 Temperature-dependent X-band EPR of IDS-oxidized (A) $^{\Delta H\Delta Z}NifD_2K_2$ and (B) $^{\Delta H\Delta Z}NifD_2K_2W_2$. Spectra were collected using 1 mW power at 9.65 GHz. All spectra are normalized for power, gain, collection time, and temperature. The signals appearing in the low-field region are provided as insets.

values (1.971, 1.951, 1.898).[51–53] While the observed inflections in the IDS-oxidized $^{\Delta H\Delta Z}NifD_2K_2$ and $^{\Delta H\Delta Z}NifD_2K_2W_2$ spectra display very similar *g*-values, the intensity ratios of these components and their temperature dependence are distinct (Fig. 8). These additional inflections are generally indicative of a spin–spin coupled system with non-integer $S > 1/2$. The presence of spin–spin coupling is consistent with our observations of the DT-reduced species.

Discussion

The nitrogenase MoFe protein from *A. vinelandii*, designated here as $NifD_2K_2$, contains two complex metalloclusters: the P-cluster and the FeMo-cofactor. Although both clusters share similar topological features, their assembly pathways differ significantly. The biosynthesis of FeMo-co does not occur on $NifD_2K_2$; instead, it is maturated on other scaffolds, and once complete inserted into an apo-form of $NifD_2K_2$ containing mature P-clusters.[9] In contrast, maturation of individual P-clusters is proposed to occur *in situ*, *via* the fusion of two distinct [4Fe:4S] clusters already contained within apposing NifDK subunits through a process involving the $NifD_2K_2$ catalytic partner, $NifH_2$, and MgATP.[18] In *A. vinelandii*, $NifD_2K_2$ sequentially binds the accessory proteins NafH, NifW and NifZ prior to the final maturation step completed by $NifH_2$.[13] Support for the [4Fe:4S] cluster fusion model has come from a variety of spectroscopic characterizations of $NifD_2K_2$ produced in the absence of $NifH_2$ ($^{\Delta H}NifD_2K_2$), which contain immature P-clusters but lack FeMo-co.[16–18,23,54]

Previous X-band perpendicular mode EPR characterization of the immature P-clusters contained in $^{\Delta H}NifD_2K_2$ revealed a mixture of two $S = 1/2$ electronic isomers with similar *g*-tensors ($g \sim$ [2.06, 1.93, 1.89] and [2.03, 1.93, 1.86]).[13,14,16] A similar signature was also observed for $NifD_2K_2$ produced in the absence of NifZ ($^{\Delta Z}NifD_2K_2$).[14] Recent biochemical studies established that both $^{\Delta H}NifD_2K_2$ and $^{\Delta Z}NifD_2K_2$ isolated by single-step affinity purification represent mixed populations of $NifD_2K_2$.[13,14] Specifically, $^{\Delta H}NifD_2K_2$ was found to be separately bound to either NafH, NifW, or NifZ, or unbound. Meanwhile, $^{\Delta Z}NifD_2K_2$ was resolved into three fractions, namely unbound, or with one or two associated NifW ($^{\Delta Z}NifD_2K_2W$ and $^{\Delta Z}NifD_2K_2W_2$, respectively). Importantly, the $^{\Delta Z}NifD_2K_2W_2$ fraction was found to be highly enriched in one of the $S = 1/2$ signals ($g \sim$ [2.03, 1.93, 1.86]), and did not exhibit the $S = 3/2$ signal associated with FeMo-co. This result indicated that the two $S = 1/2$ electronic isomers observed in $^{\Delta H}NifD_2K_2$ and $^{\Delta Z}NifD_2K_2$ represented a mixture of two different populations of immature P-cluster.

In the present work, we have shown that a strain with both *nifH* and *nifZ* gene deletions has enabled the isolation of sub-populations of immature $^{\Delta H\Delta Z}NifD_2K_2$ and $^{\Delta H\Delta Z}NifD_2K_2W_2$, each harboring immature P-clusters which are differentiable by their respective EPR signatures. As described below, isolation of these species permitted the detailed spectroscopic analysis of the immature P-cluster states associated with the corresponding samples.

Perpendicular-mode X-band EPR measurements demonstrated that a combination of the individual immature P-cluster species respectively contained in $^{\Delta H\Delta Z}NifD_2K_2$ and $^{\Delta H\Delta Z}NifD_2K_2W_2$ species recapitulates the complex EPR signature found in mixed species contained in either $^{\Delta H}NifD_2K_2$ and $^{\Delta Z}NifD_2K_2$ samples prior to their fractionation (Fig. S1†). Thus, this complex signature represents at least two distinct populations having two different states of immature P-clusters, rather than arising from individual sub-clusters or oscillating conformations contained within a single immature P-cluster species. Measurements of the Fe K-edge XAS permitted assignment of redox states of the clusters observed in each species. Both reduced samples of $^{\Delta H\Delta Z}NifD_2K_2$ and $^{\Delta H\Delta Z}NifD_2K_2W_2$ displayed a [$6Fe^{II}2Fe^{III}$] oxidation state, consistent with the presence of two $[4Fe:4S]^+$ cubanes as evidenced by EPR. Oxidation with IDS lead to the one-electron oxidation of either species, which suggests that only one subcluster within an individual P-cluster precursor is oxidized to $[4Fe:4S]^{2+}$ while the other maintains its valency, indicating different redox properties for each subcluster. In contrast, IDS treatment of mature, all-ferrous P-cluster (P^N) results in a two-electron oxidation to form P^{2+}, shifting from an $[8Fe:7S]^0$ state to a $[8Fe:7S]^{2+}$ state, consistent with previous measurements.[25]

EPR simulations of reduced $^{\Delta H\Delta Z}NifD_2K_2$ and $^{\Delta H\Delta Z}NifD_2K_2W_2$, combined with spin quantification, suggest their

corresponding spectra represent two unique $S = 1/2$ species having similar electronic properties arising from two distinct [4Fe:4S] clusters. Weak spin-coupling detected *via* parallel-mode X-band EPR further supports that these two species are spatially close enough to display spin–spin coupling. This coupling is significantly increased in the $^{\Delta H\Delta Z}NifD_2K_2W_2$ sample when compared to $^{\Delta H\Delta Z}NifD_2K_2$, suggesting a decrease in distance between the two $[4Fe:4S]^+$ cubanes in the NifW bound state, and hence an associated conformational change in $^{\Delta H\Delta Z}NifD_2K_2$ upon binding of NifW. Spin–spin coupling is also observed in equivalent oxidized samples, again differing between $^{\Delta H\Delta Z}NifD_2K_2$ and $^{\Delta H\Delta Z}NifD_2K_2W_2$. The unique spectra of these oxidized samples are reminiscent of open [4Fe:4S] clusters, albeit with significantly different temperature-dependent behavior.[51–53,55]

Despite having similar electronic properties, the immature P-clusters contained in $^{\Delta H\Delta Z}NifD_2K_2$ and $^{\Delta H\Delta Z}NifD_2K_2W_2$ display significant structural differences, as indicated in our XAS analyses by both shifts in the intensity and energetic position of the pre-edge feature and by variations in the EXAFS region. Remarkably, EXAFS analysis of $^{\Delta H\Delta Z}NifD_2K_2W_2$ suggests additional Fe-coordination of 1–2 light atom(s) (N or O) per [4Fe:4S] subcluster when compared to the $^{\Delta H\Delta Z}NifD_2K_2$ species, even when regarding stringent considerations of fitting statistics. This observation suggests a transition or stabilization of the coordination environment for one or, perhaps, both subclusters upon NifW binding.

It should be noted that although this work has revealed that $NifD_2K_2$ from cells deleted for the *nifH* and *nifZ* genes represents a pool of two distinct $^{\Delta H\Delta Z}NifD_2K_2$ and $^{\Delta H\Delta Z}NifD_2K_2W_2$ species, this does not necessarily indicate that either species accumulates significantly under normal physiological conditions. The $^{\Delta H\Delta Z}NifD_2K_2$ species lacking bound NifW may accumulate due to interruption of the maturation process in the absence of NifZ and $NifH_2$. Both transcriptomic and proteomic studies have revealed that NifD and NifK are expressed and accumulate *in vivo* at much higher levels than the NafH, NifW, and NifZ assembly factors.[56,57] Consequently, when the maturation process is interrupted by the inactivation of NifZ and $NifH_2$, the available NifW would become sequestered into a $NifD_2K_2W_2$ complex, and excess immature $NifD_2K_2$ lacking NifW would be forced to accumulate. In contrast, under physiological conditions maturation must occur more rapidly than assembly intermediates can accumulate. Hence, deleting genes involved in P-cluster maturation offers biochemical snapshots of this process. In this context, $^{\Delta H\Delta Z}NifD_2K_2W_2$ allows the characterization of the NifDKW complex occurring in physiological conditions, and $^{\Delta H\Delta Z}NifD_2K_2$ represents an immature $NifD_2K_2$ species prior to interaction with NifW.

Conclusions

Taken together, our results shed light on the structure of the individual immature P-cluster states and on the possible roles of NifW. Upon binding of NifW to $^{\Delta H\Delta Z}NifD_2K_2$, a decrease in the distance between both $[4Fe:4S]^+$ clusters occurs along with the coordination of 2–4 light atoms (O or N) per [8Fe:8S] unit. The combination of these observations supports a NifW-instigated conformational change in the $NifD_2K_2$ at the NifD/NifK subunit interface to assist in cubane fusion. A conformational role for NifW in optimizing a configuration of NifD and NifK to promote efficient P-cluster maturation is consistent with the observation that loss of NifW function only results in the lower accumulation of active $NifD_2K_2$ that displays the characteristic EPR signature associated with FeMo-co.[22] The possible participation of assembly factors such as NafH and NifW in promoting subunit interaction has previously been indicated by studies that have demonstrated both NifD and NifK can accumulate in the absence of each other, and that crude extracts harbouring separately produced NifD or NifK can be mixed to achieve only a very low level of activity.[58] Nevertheless, NifD- and NifK-subunits produced in the absence of each other have yet to be purified and characterized. In our current working model, NifW conformationally assists the fusion of the two subclusters in a pathway that also involves NifZ, $NifH_2$ and MgATP. In this provisional model, NifZ is proposed to assist dissociation of NifW from the $NifD_2K_2W_2$ complex and, possibly recruit $NifH_2$ to support sub-cluster fusion. In support of this model an interaction between NifW and NifZ, based on yeast-two-hybrid studies has been suggested.[59]

An analogous example of [4Fe:4S] cluster fusion following slight structural changes has also been recently reported for formation of a stable [8Fe:8S] precursor of FeMo-co, the K-cluster.[11] Strikingly, the ligand environment of the K-cluster appears identical to that of the P-cluster, underlining a structural convergence for [4Fe:4S] cluster fusion. Formation of P-clusters directly within an immature form of $NifD_2K_2$ represents a fundamentally different pathway than completion of FeMo-co formation prior to its insertion into an apo-form of $NifD_2K_2$ that already contains intact P-clusters. Nevertheless, P-clusters and FeMo-co share striking topological similarities and a common mechanistic feature in their respective assemblies involving reductant-dependent fusion of subclusters. Further studies are required to fully elucidate the conformational changes which occur upon binding of NifW to $NifD_2K_2$ – namely, structural resolution *via* crystallography could determine the structural changes occurring around the clusters.

Data availability

Additional data and parameters regarding spectral fitting are available in the ESI file.† Further data may be furnished upon request.

Author contributions

C. V. S. and E. J. V. contributed equally to this work. C. V. S., E. J.-V., L. D. and D. R. D. conceived and supervised the project. C. V. S., E. J.-V., A. P.-G. and Z.-Y. Y. acquired and analysed the data. C. V. S. and L. D. wrote the draft. All authors participated in manuscript preparation and draft revision before the final submission.

Conflicts of interest

There are no conflicts to declare.

Acknowledgements

C. V. S., S. D., and L. D. would like to thank the Max-Planck Society for funding. S. D. and C. V. S. acknowledge the DFG SPP 1927 "Iron–Sulfur for Life" (project DE 1877/1-1) for funding. L. D. thanks the Peter und Traudl Engelhorn Stiftung for funding. Use of the Stanford Synchrotron Radiation Lightsource, SLAC National Accelerator Laboratory, was supported by the U.S. Department of Energy, Office of Science, Office of Basic Energy Sciences under Contract No. DE-AC02-76SF00515. C. V. S., S. D., and L. D. gratefully acknowledge Matthew Latimer for his technical assistance during XAS measurements at beamline 9-3. George E. Cutsail III, Justin H. Henthorn, and Patricia Rodríguez Macía are also thanked for their assistance in XAS data collection. E. J.-V. and A. P. G. were supported by Bill and Melinda Gates Foundation grants BNF Cereals Phase II (OPP1143172) and BNF Cereals Phase III (INV-005889). Work in the laboratories of L. C. S and D. R. D. is supported by grants from the U.S. Department of Energy, Office of Science, Basic Energy Science, DE-SC0010834 and DE-SC0010867, respectively. This work was supported, in whole or in part, by the Bill & Melinda Gates Foundation (OPP1143172, INV-005889). Under the grant conditions of the Foundation, a Creative Commons Attribution 4.0 Generic License has already been assigned to the Author Accepted Manuscript version that might arise from this submission.

Notes and references

§ $NifD_2K_2$ isolated from a particular genetic background in which gene-encoding components involved in maturation have been deleted are indicated by a superscript. For example, $NifD_2K_2$ isolated from a strain deleted for the gene encoding NifH is indicated as $^{\Delta H}NifD_2K_2$.

1 L. C. Seefeldt, Z. Y. Yang, D. A. Lukoyanov, D. F. Harris, D. R. Dean, S. Raugei and B. M. Hoffman, Reduction of Substrates by Nitrogenases, *Chem. Rev.*, 2020, **120**(12), 5082.
2 C. Van Stappen, L. Decamps, G. E. Cutsail 3rd, R. Bjornsson, J. T. Henthorn, J. A. Birrell and S. DeBeer, The Spectroscopy of Nitrogenases, *Chem. Rev.*, 2020, **120**(12), 5005.
3 O. Einsle and D. C. Rees, Structural Enzymology of Nitrogenase Enzymes, *Chem. Rev.*, 2020, **120**(12), 4969.
4 M. A. Addo and P. C. Dos Santos, Distribution of Nitrogen-Fixation Genes in Prokaryotes Containing Alternative Nitrogenases, *ChemBioChem*, 2020, **21**(12), 1749.
5 J. W. Peters, K. Fisher, W. E. Newton and D. R. Dean, Involvement of the P-Cluster in Intramolecular Electron-Transfer within the Nitrogenase MoFe Protein, *J. Biol. Chem.*, 1995, **270**(45), 27007.
6 J. M. Chan, J. Christiansen, D. R. Dean and L. C. Seefeldt, Spectroscopic evidence for changes in the redox state of the nitrogenase P-cluster during turnover, *Biochemistry*, 1999, **38**(18), 5779.
7 N. Xiang, C. Y. Guo, J. W. Liu, H. Xu, R. Dixon, J. G. Yang and Y. P. Wang, Using synthetic biology to overcome barriers to stable expression of nitrogenase in eukaryotic organelles, *Proc. Natl. Acad. Sci. U. S. A.*, 2020, **117**(28), 16537.
8 S. Okada, C. M. Gregg, R. S. Allen, A. Menon, D. Hussain, V. Gillespie, E. Johnston, K. Byrne, M. L. Colgrave and C. C. Wood, A Synthetic Biology Workflow Reveals Variation in Processing and Solubility of Nitrogenase Proteins Targeted to Plant Mitochondria, and Differing Tolerance of Targeting Sequences in a Bacterial Nitrogenase Assay, *Front. Plant Sci.*, 2020, **11**, 552160.
9 S. Buren, E. Jimenez-Vicente, C. Echavarri-Erasun and L. M. Rubio, Biosynthesis of Nitrogenase Cofactors, *Chem. Rev.*, 2020, **120**(12), 4921.
10 G. Lopez-Torrejon, S. Buren, M. Veldhuizen and L. M. Rubio, Biosynthesis of cofactor-activatable iron-only nitrogenase in *Saccharomyces cerevisiae*, *Microb. Biotechnol.*, 2021, **14**(3), 1073.
11 L. P. Jenner, M. V. Cherrier, P. Amara, L. M. Rubio and Y. Nicolet, An unexpected P-cluster like intermediate en route to the nitrogenase FeMo-co, *Chem. Sci.*, 2021, **12**, 5269–5274.
12 J. Christiansen, P. J. Goodwin, W. N. Lanzilotta, L. C. Seefeldt and D. R. Dean, Catalytic and biophysical properties of a nitrogenase Apo-MoFe protein produced by a nifB-deletion mutant of *Azotobacter vinelandii*, *Biochemistry*, 1998, **37**(36), 12611.
13 E. Jimenez-Vicente, Z. Y. Yang, W. K. Ray, C. Echavarri-Erasun, V. L. Cash, L. M. Rubio, L. C. Seefeldt and D. R. Dean, Sequential and differential interaction of assembly factors during nitrogenase MoFe protein maturation, *J. Biol. Chem.*, 2018, **293**(25), 9812.
14 E. Jimenez-Vicente, Z. Y. Yang, J. S. Martin Del Campo, V. L. Cash, L. C. Seefeldt and D. R. Dean, The NifZ accessory protein has an equivalent function in maturation of both nitrogenase MoFe protein P-clusters, *J. Biol. Chem.*, 2019, **294**(16), 6204.
15 J. W. Peters, M. H. Stowell, S. M. Soltis, M. G. Finnegan, M. K. Johnson and D. C. Rees, Redox-dependent structural changes in the nitrogenase P-cluster, *Biochemistry*, 1997, **36**(6), 1181.
16 M. W. Ribbe, Y. Hu, M. Guo, B. Schmid and B. K. Burgess, The FeMoco-deficient MoFe protein produced by a *nifH* deletion strain of *Azotobacter vinelandii* shows unusual P-cluster features, *J. Biol. Chem.*, 2002, **277**(26), 23469.
17 M. C. Corbett, Y. Hu, F. Naderi, M. W. Ribbe, B. Hedman and K. O. Hodgson, Comparison of iron–molybdenum cofactor-deficient nitrogenase MoFe proteins by X-ray absorption spectroscopy: implications for P-cluster biosynthesis, *J. Biol. Chem.*, 2004, **279**(27), 28276.
18 Y. Hu, A. W. Fay, C. C. Lee and M. W. Ribbe, P-cluster maturation on nitrogenase MoFe protein, *Proc. Natl. Acad. Sci. U. S. A.*, 2007, **104**(25), 10424.
19 A. C. Robinson, D. R. Dean and B. K. Burgess, Iron–molybdenum cofactor biosynthesis in *Azotobacter vinelandii* requires the iron protein of nitrogenase, *J. Biol. Chem.*, 1987, **262**(29), 14327.

20 A. C. Robinson, T. W. Chun, J. G. Li and B. K. Burgess, Iron–Molybdenum Cofactor Insertion into the Apo-MoFe Protein of Nitrogenase Involves the Iron Protein-MgATP Complex, *J. Biol. Chem.*, 1989, **264**(17), 10088.

21 M. R. Jacobson, V. L. Cash, M. C. Weiss, N. F. Laird, W. E. Newton and D. R. Dean, Biochemical and genetic analysis of the nifUSVWZM cluster from *Azotobacter vinelandii*, *Mol. Gen. Genet.*, 1989, **219**(1–2), 49.

22 S. Kim and B. K. Burgess, Evidence for the direct interaction of the *nifW* gene product with the MoFe protein, *J. Biol. Chem.*, 1996, **271**(16), 9764.

23 N. Gavini, L. Ma, G. Watt and B. K. Burgess, Purification and characterization of a FeMo cofactor-deficient MoFe protein, *Biochemistry*, 1994, **33**(39), 11842.

24 C. Van Stappen, A. T. Thorhallsson, L. Decamps, R. Bjornsson and S. DeBeer, Resolving the structure of the E1 state of Mo nitrogenase through Mo and Fe K-edge EXAFS and QM/MM calculations, *Chem. Sci.*, 2019, **10**(42), 9807.

25 K. B. Musgrave, H. I. Liu, L. Ma, B. K. Burgess, G. Watt, B. Hedman and K. O. Hodgson, EXAFS studies on the P^N and P^{OX} states of the P-clusters in nitrogenase, *JBIC, J. Biol. Inorg. Chem.*, 1998, **3**(4), 344.

26 K. B. Musgrave, H. C. Angove, B. K. Burgess, B. Hedman and K. O. Hodgson, All-ferrous titanium(III) citrate reduced Fe protein of nitrogenase: An XAS study of electronic and metrical structure, *J. Am. Chem. Soc.*, 1998, **120**(21), 5325.

27 J. K. Kowalska, A. W. Hahn, A. Albers, C. E. Schiewer, R. Bjornsson, F. A. Lima, F. Meyer and S. DeBeer, X-ray Absorption and Emission Spectroscopic Studies of $[L_2Fe_2S_2]_{(n)}$ Model Complexes: Implications for the Experimental Evaluation of Redox States in Iron–Sulfur Clusters, *Inorg. Chem.*, 2016, **55**(9), 4485.

28 G. R. Shulman, Y. Yafet, P. Eisenberger and W. E. Blumberg, Observations and interpretation of X-ray absorption edges in iron compounds and proteins, *Proc. Natl. Acad. Sci. U. S. A.*, 1976, **73**(5), 1384.

29 H. P. Hanson and J. R. Knight, X-Ray Absorption Edges of Transition Metal Salts, *Phys. Rev.*, 1956, **102**(3), 632.

30 A. J. Pierik, H. Wassink, H. Haaker and W. R. Hagen, Redox properties and EPR spectroscopy of the P clusters of *Azotobacter vinelandii* MoFe protein, *Eur. J. Biochem.*, 1993, **212**(1), 51.

31 J. Christiansen, R. C. Tittsworth, B. J. Hales and S. P. Cramer, Fe and Mo EXAFS of *Azotobacter vinelandii* Nitrogenase in Partially Oxidized and Singly Reduced Forms, *J. Am. Chem. Soc.*, 1995, **117**(40), 10017.

32 H. L. Rutledge, J. Rittle, L. M. Williamson, W. A. Xu, D. M. Gagnon and F. A. Tezcan, Redox-Dependent Metastability of the Nitrogenase P-Cluster, *J. Am. Chem. Soc.*, 2019, **141**(25), 10091.

33 T. Spatzal, M. Aksoyoglu, L. Zhang, S. L. Andrade, E. Schleicher, S. Weber, D. C. Rees and O. Einsle, Evidence for interstitial carbon in nitrogenase FeMo cofactor, *Science*, 2011, **334**(6058), 940.

34 J. M. Berg, K. O. Hodgson and R. H. Holm, Crystal-Structure of $[(C_2H_5)4n]3[Fe_4S_4(Sch2ph)_4]$, a Reduced Ferredoxin Site Analog with a Nontetragonal Fe_4S_4 Core Structure in the Solid-State, *J. Am. Chem. Soc.*, 1979, **101**(16), 4586.

35 C. R. Sharp, J. S. Duncan and S. C. Lee, $[Fe_{(4)}S_{(4)}]_{(q)}$ cubane clusters (q = 4+, 3+, 2+) with terminal amide ligands, *Inorg. Chem.*, 2010, **49**(14), 6697.

36 Y. Ohki, K. Tanifuji, N. Yamada, M. Imada, T. Tajima and K. Tatsumi, Synthetic analogues of $[Fe_4S_4(Cys)3(His)]$ in hydrogenases and $[Fe_4S_4(Cys)_4]$ in HiPIP derived from all-ferric $[Fe_4S_4\{N(SiMe_3)_2\}_4]$, *Proc. Natl. Acad. Sci. U. S. A.*, 2011, **108**(31), 12635.

37 G. Moula, T. Matsumoto, M. E. Miehlich, K. Meyer and K. Tatsumi, Synthesis of an All-Ferric Cuboidal Iron–Sulfur Cluster $[Fe(III)_4S_4(SAr)_4]$, *Angew. Chem., Int. Ed. Engl.*, 2018, **57**(36), 11594.

38 B. B. Wenke, T. Spatzal and D. C. Rees, Site-Specific Oxidation State Assignments of the Iron Atoms in the [4Fe:4S](2+/1+/0) States of the Nitrogenase Fe–Protein, *Angew. Chem., Int. Ed. Engl.*, 2019, **58**(12), 3894.

39 P. A. Lindahl, E. P. Day, T. A. Kent, W. H. Orme-Johnson and E. M. Munck, EPR, and magnetization studies of the Azotobacter vinelandii Fe protein. Evidence for a $[4Fe–4S]^{1+}$ cluster with spin S = 3/2, *J. Biol. Chem.*, 1985, **260**(20), 11160.

40 M. J. Carney, G. C. Papaefthymiou, K. Spartalian, R. B. Frankel and R. H. Holm, Ground spin state variability in $[Fe_4S_4(SR)_4]^{3-}$. Synthetic analogs of the reduced clusters in ferredoxins and other iron–sulfur proteins: cases of extreme sensitivity of electronic state and structure to extrinsic factors, *J. Am. Chem. Soc.*, 1988, **110**(18), 6084.

41 D. H. Flint, M. H. Emptage and J. R. Guest, Fumarase-a from *Escherichia coli* – Purification and Characterization as an Iron–Sulfur Cluster Containing Enzyme, *Biochemistry*, 1992, **31**(42), 10331.

42 E. C. Duin, M. E. Lafferty, B. R. Crouse, R. M. Allen, I. Sanyal, D. H. Flint and M. K. Johnson, [2Fe–2S] to [4Fe–4S] cluster conversion in *Escherichia coli* biotin synthase, *Biochemistry*, 1997, **36**(39), 11811.

43 W. R. Hagen, R. R. Eady, W. R. Dunham and H. Haaker, A novel $S = 3/2$ EPR signal associated with native Fe-proteins of nitrogenase, *FEBS Lett.*, 1985, **189**(2), 250.

44 M. Hans, W. Buckel and E. Bill, The iron–sulfur clusters in 2-hydroxyglutaryl-CoA dehydratase from Acidaminococcus fermentans. Biochemical and spectroscopic investigations, *Eur. J. Biochem.*, 2000, **267**(24), 7082.

45 H. Rupp, R. Cammack, K. K. Rao and D. O. Hall, Electron-Spin Relaxation of Iron–Sulfur Proteins Studied by Microwave-Power Saturation, *Biochim. Biophys. Acta*, 1978, **537**(2), 255.

46 R. Aasa and T. Vanngard, Epr Signal Intensity and Powder Shapes – Re-Examination, *J. Magn. Reson.*, 1975, **19**(3), 308.

47 C. Riplinger, J. P. Kao, G. M. Rosen, V. Kathirvelu, G. R. Eaton, S. S. Eaton, A. Kutateladze and F. Neese, Interaction of radical pairs through-bond and through-space: scope and limitations of the point-dipole approximation in electron paramagnetic resonance spectroscopy, *J. Am. Chem. Soc.*, 2009, **131**(29), 10092.

48 K. K. Surerus, M. P. Hendrich, P. D. Christie, D. Rottgardt, W. H. Ormejohnson and E. Munck, Mossbauer and

Integer-Spin Epr of the Oxidized P-Clusters of Nitrogenase – Pox Is a Non-Kramers System with a Nearly Degenerate Ground Doublet, *J. Am. Chem. Soc.*, 1992, **114**(22), 8579.

49 C. P. Owens, F. E. Katz, C. H. Carter, V. F. Oswald and F. A. Tezcan, Tyrosine-Coordinated P-Cluster in *G. diazotrophicus* Nitrogenase: Evidence for the Importance of O-Based Ligands in Conformationally Gated Electron Transfer, *J. Am. Chem. Soc.*, 2016, **138**(32), 10124.

50 W. R. Hagen, W. R. Dunham, M. K. Johnson and J. A. Fee, Quarter field resonance and integer-spin/half-spin interaction in the EPR of *Thermus thermophilus* ferrodoxin. Possible new fingerprints for three iron clusters, *Biochim. Biophys. Acta, Protein Struct. Mol. Enzymol.*, 1985, **828**(3), 369.

51 W. R. Hagen, A. J. Pierik and C. Veeger, Novel electron paramagnetic resonance signals from an Fe/S protein containing six iron atoms, *J. Chem. Soc., Faraday Trans. 1*, 1989, **85**(12), 4083.

52 A. J. Pierik, W. R. Hagen, W. R. Dunham and R. H. Sands, Multi-frequency EPR and high-resolution Mossbauer spectroscopy of a putative [6Fe–6S] prismane-cluster-containing protein from *Desulfovibrio vulgaris* (Hildenborough). Characterization of a supercluster and superspin model protein, *Eur. J. Biochem.*, 1992, **206**(3), 705.

53 W. R. Hagen, Structure and function of the hybrid cluster protein, *Coord. Chem. Rev.*, 2022, **457**, 214405.

54 R. B. Broach, K. Rupnik, Y. L. Hu, A. W. Fay, M. Cotton, M. W. Ribbe and B. J. Hales, Variable-temperature, variable-field magnetic circular dichroism spectroscopic study of the metal clusters in the Delta *nifB* and Delta *nifH* MoFe proteins of nitrogenase from *Azotobacter vinelandii*, *Biochemistry*, 2006, **45**(50), 15039.

55 M. M. Roessler, R. M. Evans, R. A. Davies, J. Harmer and F. A. Armstrong, EPR spectroscopic studies of the Fe–S clusters in the O_2-tolerant [NiFe]-hydrogenase Hyd-1 from *Escherichia coli* and characterization of the unique [4Fe–3S] cluster by HYSCORE, *J. Am. Chem. Soc.*, 2012, **134**(37), 15581.

56 T. L. Hamilton, M. Jacobson, M. Ludwig, E. S. Boyd, D. A. Bryant, D. R. Dean and J. W. Peters, Differential accumulation of nif structural gene mRNA in *Azotobacter vinelandii*, *J. Bacteriol.*, 2011, **193**(17), 4534.

57 C. Poza-Carrion, E. Jimenez-Vicente, M. Navarro-Rodriguez, C. Echavarri-Erasun and L. M. Rubio, Kinetics of Nif gene expression in a nitrogen-fixing bacterium, *J. Bacteriol.*, 2014, **196**(3), 595.

58 A. C. Robinson, B. K. Burgess and D. R. Dean, Activity, Reconstitution, and Accumulation of Nitrogenase Components in *Azotobacter vinelandii* Mutant Strains Containing Defined Deletions within the Nitrogenase Structural Gene-Cluster, *J. Bacteriol.*, 1986, **166**(1), 180.

59 S. H. Lee, L. Pulakat, K. C. Parker and N. Gavini, Genetic analysis on the NifW by utilizing the yeast two-hybrid system revealed that the NifW of *Azotobacter vinelandii* interacts with the NifZ to form higher-order complexes, *Biochem. Biophys. Res. Commun.*, 1998, **244**, 498.